ADVANCED MATERIALS
www.advmat.de

Ultrahigh-Performance Solar-Blind Photodetectors Based on Individual Single-crystalline $In_2Ge_2O_7$ Nanobelts

By *Liang Li,* Pooi See Lee, Chaoyi Yan, Tianyou Zhai,* Xiaosheng Fang,* Meiyong Liao,* Yasuo Koide, Yoshio Bando,* and *Dmitri Golberg*

Deep-ultraviolet (DUV) photodetectors working in the solar-blind spectrum range (220–290 nm) have received significant attention, because of various important applications in missile tracking, flame detection, ozone layer monitoring, and so on.[1–3] To date, DUV solar-blind photodetectors based on wide bandgap semiconductors, e.g., AlGaN, ZnMgO, $LaAlO_3$, BN, and diamond films, have been explored. However, their fabrication processes are complex and costly, and it is difficult to produce single-crystals of these materials owing to phase-separation and lattice mismatch with substrates, which result in a responsivity <1 and a quantum efficiency $<10^2$%.[4,5]

Recently, one-dimensional (1D) nanostructures have been widely studied to enhance the quantum efficiency and shorten the response time of photodetectors. This approach originates from the large surface-to-volume ratio and low dimensionality in 1D structures.[6–9] Among these detectors, solar-blind ones have received little attention.[10] Moreover, their response and decay times are still long, and their responsivity and quantum efficiency are not high enough. Therefore, we undertook a challenge to develop high-performance solar-blind nanometer-scale photodetectors in the present work.

Ternary oxide $In_2Ge_2O_7$ bulk forms are important materials for catalysts, ion exchange, humidity sensors, and high energy laser systems.[11] Several 1D $In_2Ge_2O_7$ nanostructures, such as nanowires, nanoribbons, and nanotubes, have been synthesized,[12] but properties have seldom been reported[12b] and possible applications have not been exploited. In this communication, we first report on the fabrication of ultrahigh-performance solar-blind photodetectors employing individual single-crystalline $In_2Ge_2O_7$ nanobelts as sensing elements. Such photodetectors show a sensitive spectral response, a significantly shortened response, and decay times of ~3 ms, compared with the characteristic parameters of the pre-existing devices (order of approx. seconds), and a high quantum efficiency, i.e., nearly six orders of magnitude higher than reported before. Our results imply that an $In_2Ge_2O_7$ nanobelt can be an excellent candidate for high-speed and high-sensitivity photodetectors or optical switches.

Morphology, crystal structure, and spatially resolved maps of as-prepared $In_2Ge_2O_7$ nanobelts are shown in **Figure 1**. A typical scanning electron microscopy (SEM) image in Figure 1a reveals that the nanobelts are up to hundreds of micrometers in length. The widths and thicknesses have a size distribution of 250 nm to 3 μm and 10–50 nm, respectively. The X-ray diffraction (XRD) peaks (Figure S1) can be indexed to a pure monoclinic $In_2Ge_2O_7$ crystal phase (JCPDS: 82-0846). A high-resolution transmission electron microscopy (HRTEM) image (Figure 1b) demonstrates clearly the belt morphology. The corresponding lattice fringe image indicates the single-crystalline character of the belts. The interplanar *d*-spacing of 0.45 nm corresponds to the (010) lattice plane of monoclinic $In_2Ge_2O_7$, indicating a preferred [010] growth direction. The elemental maps displayed in Figure 1c–f demonstrate a uniform distribution of the compositional elements In, Ge, and O. Therefore, high-quality single-crystalline $In_2Ge_2O_7$ nanobelts have been fabricated.

The configuration of a photoconductive device for the photoresponse measurement on an individual nanobelt is shown in the inset of **Figure 2a**. A monochromatic light was illuminated on the nanobelt connected by one pair of Cr/Au electrodes, and the photoresponse was measured by using a two-probe method. The SEM image of an individual nanobelt (width 270 nm, thickness 30 nm, and length 2.7 μm) device is inserted in Figure 2c (an enlarged image is shown in Figure S2). Figure 2a represents a spectral response of the $In_2Ge_2O_7$-nanobelt photodetector at a 3.0 V bias at room temperature. The photodetector shows a high sensitivity to DUV light with a cutoff wavelength of ~290 nm, which corresponds to a photon energy that is close to the bandgap (4.43 eV, 280 nm) of $In_2Ge_2O_7$,[13] which implies a bandgap excitation related process. To further analyze the selectivity of the photodetector to a wavelength, the logarithmic plot of Figure 2a is shown in Figure 2b. As expected, with decreasing the wavelength (increasing the phonon energy), the responsivity increases gradually and reaches a maximum value at ~230 nm. This wavelength is consistent with the maximum absorption peak ~244 nm in the optical absorption spectrum (the inset in Figure 2b). It is worth noting that the responsivity at 230 nm is 2–3 and 3–6 orders of magnitude higher than that in the ultraviolet and visible light ranges, respectively, which indicates high selectivity towards the solar-blind light. Figure 2c shows the *I–V* curves of the $In_2Ge_2O_7$-nanobelt photodetector exposed to 230 nm light or under dark conditions.

[*] Dr. L. Li, Dr. T. Y. Zhai, Dr. X. S. Fang, Prof. Y. Bando, Prof. D. Golberg
International Center for Materials Nanoarchitectonics (MANA)
National Institute for Materials Science (NIMS)
Namiki 1–1, Tsukuba, Ibaraki, 305–0044 (Japan)
E-mail: LI.Liang@nims.go.jp; ZHAI.Tianyou@nims.go.jp;
FANG.Xiaosheng@nims.go.jp
Prof. P. S. Lee, Dr. C. Y. Yan
School of Materials Science and Engineering
Nanyang Technological University (NTU) (Singapore)
Dr. M. Y. Liao, Prof. Y. Koide
Sensor Materials Center, NIMS
Namiki 1–1, Tsukuba, Ibaraki, 305–0044 (Japan)
E-mail: Meiyong.Liao@nims.go.jp

DOI: 10.1002/adma.201002608

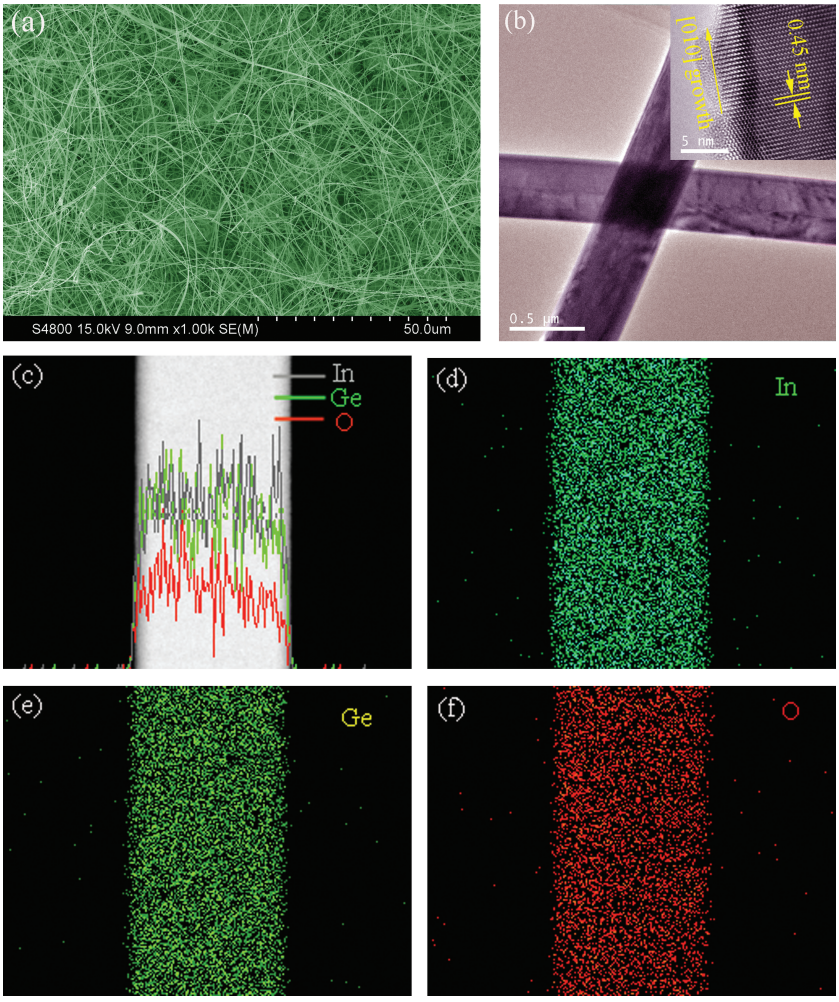

Figure 1. a) SEM image of numerous $In_2Ge_2O_7$ nanobelts. b) TEM image of individual $In_2Ge_2O_7$ nanobelts, and corresponding HRTEM image. c) Line-scan profile across the radial direction of an individual nanobelt. d), e) and f) In, Ge and O elemental maps, respectively.

The linear *I*–*V* characteristics indicate the good ohmic contacts between the nanobelt and electrodes. A high photo-excited current of ~19 nA was recorded at a low bias of 5.0 V. A corresponding logarithmic plot (Figure 2d) clearly shows that the photo-excited current significantly increases by six orders of magnitude compared with a low dark current, indicating a high sensitivity.

The time-dependent photoresponse of the $In_2Ge_2O_7$-nanobelt photodetector was measured by periodically turning on and off 230 nm light with a light intensity of 19 μW cm^{-2} at a bias of 10 V, as shown in **Figure 3a**. On illumination, the current rapidly increases to a stable value of ~48 nA, and then sharply returns to its initial one as the light is turned off. The photodetector shows highly stable and reproducible characteristics. From the enlarged view (Figure 3b) of one ON/OFF cycle, the response and decay times (t_r and t_d) are so short that they exceed the detection limit (0.3 s) of our direct current (dc) picoampermeter. The time taken for the current to increase from 10% to 90% of the peak value or vice versa is defined as the t_r and t_d, respectively. Under closer examination using a 230 nm light source pulse chopped at a frequency of 100 Hz, as shown in Figure 3c, both the t_r and t_d were measured to be ~2 ms. To more accurately estimate response and decay times, we decreased the collection step of the signal to 8.0 and 4.0 μs under the resolution range of our apparatus, as shown in Figure S3. All these data show that the response and decay times are smaller than 3 ms.

Both the rising and decaying edges of the photocurrents can be fitted by the exponential equation $I = I_0(1 - e^{-t/\tau_r})$ and $I = I_0 e^{-t/\tau_d}$, respectively. A linear relationship between Ln*I* and *t* is obtained (Figure S4). The fitting of both the rising and decaying edges requires two straight lines of different slopes, from which different time constants (τ_{r1} and τ_{r2} are 1.30 ms and 2.70 ms; τ_{d1} and τ_{d2} are 3.23 ms and 3.70 ms) are obtained. The time constants for rising edges are smaller than those for decaying edges, but both are much larger than those usually observed for intrinsic band-to-band excitation in semiconductors (much lower than milliseconds), which indicates that traps were involved in this process.[8f] The photogenerated carriers may first fill the traps and then reach the maximum after all the traps are saturated. The relatively fast decay with the time constant of 3.23 ms is representative of the carrier lifetime.

In addition to selectivity, responsivity, and response and decay times, the quantum efficiency (QE) (defined as the number of carriers circulating through a photodetector per absorbed photon and per unit time) determines the efficiency of an electron transport and carrier collection. It is noticed that the present QE is equal to the current gain also used in the literature.[4a,9f] The QE can be expressed by: QE = $hcR_\lambda/e\lambda$, where *h* is Planck's constant, *c* is the velocity of light, *e* is the electronic charge, λ is the wavelength (230 nm) of irradiated light, and $R_\lambda = I_p/PS$ (where the photocurrent $I_p = I_{il} - I_d$, where I_d is the dark current and I_{il} is the current in the device when it is illuminated with a light source, *P* is the light intensity irradiated on the nanobelt, and *S* is the effective illuminated area). The R_λ of the present photodetector irradiated by 230 nm light at 19 μW cm^{-2} is 3.9×10^5 A W^{-1}. This corresponds to an ultrahigh QE of 2.0×10^8%. At present, these values are the best photoconductive parameters among all reported 1D nanometer-scale solar-blind photodetectors.[10]

The photoresponse of oxide semiconductors is a complex process of electron-hole generation, trapping, and recombination. Based on the quantitative expression QE = t_{life}/t_{tran} (t_{life} is the lifetime of carriers and t_{tran} is the transit time between electrodes),[8a] there are three factors that mainly affect t_{life} and t_{tran}: surface hole-trap states, confined active area, and crystal quality of sensing elements. 1) The large surface-to-volume ratio of $In_2Ge_2O_7$ nanobelts largely increases the number of surface

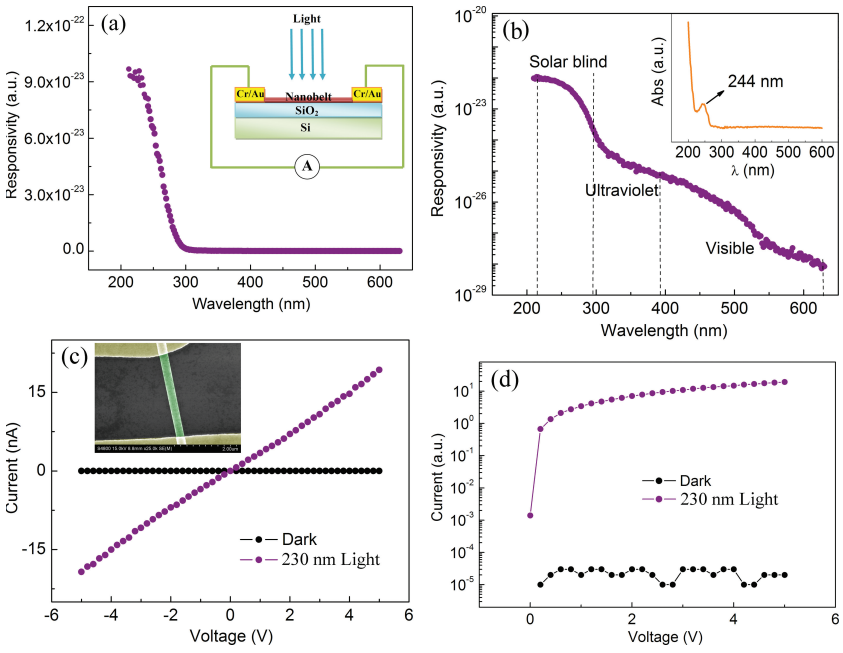

Figure 2. a) Spectral response of an individual $In_2Ge_2O_7$-nanobelt photodetector, demonstrating a cutoff wavelength (<290 nm) in the solar-blind spectrum range. The inset is a schematic of a device for measuring photoconductivity. b) Logarithmic plot of (a) revealing high sensitivity and selectivity to various light wavelengths. The optical absorption spectrum of nanobelts is inserted in the top-right corner. c) *I–V* curves of the individual $In_2Ge_2O_7$-nanobelt photodetector under 230 nm irradiation or dark conditions. The inset is a typical SEM image of an $In_2Ge_2O_7$-nanobelt device. d) Logarithmic plot of (c) shows the large ratio of photo-excited to dark current.

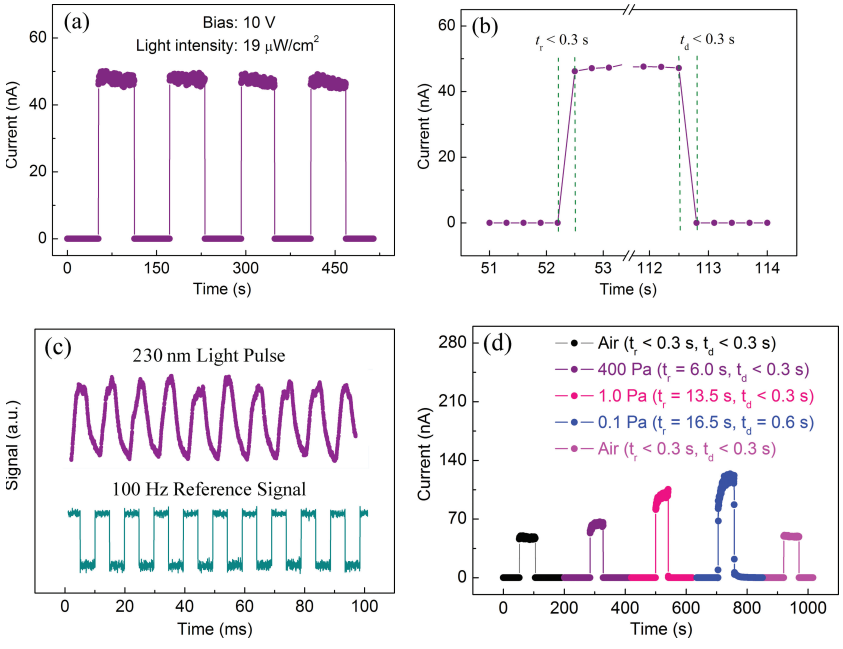

Figure 3. a) Time response of an $In_2Ge_2O_7$-nanobelt photodetector. b) The enlarged portions of the 51–53 s and 112–114 s ranges showing ultimately fast response and decay times (beyond the detection limit (0.3 s)). c) A transient response by illuminating the $In_2Ge_2O_7$-nanobelt photodetector with a 230 nm light pulse chopped at a frequency of 100 Hz with the reference signal. d) The response of a photocurrent under air and different vacuum environments.

trap states, prolonging the t_{life}.[14] In air, oxygen molecules tend to take free electrons of $In_2Ge_2O_7$ nanobelts and form negatively charged oxygen ions at the surface, which results in the surface band bending and thus creating the surface depletion areas, which decrease the density and mobility of free carriers. This trapping process further reduces the dark current in addition to the wide bandgap character of $In_2Ge_2O_7$. Upon light irradiation, electron–hole pairs are excited. The holes migrate to the surface and trap electrons from oxygen ions, changing them into oxygen molecules which then desorb from the nanobelt surface. The remaining free electrons contribute to a photocurrent. This hole-trapping process effectively separates electron–hole pairs and largely increases the t_{life}, which can be confirmed by a current response to ambient conditions measured under 230 nm light irradiation at 19 μW cm^{-2} (Figure 3d). It can be seen that the current increases as the ambient changes from air to vacuum, and continuously increases with decreasing pressure from 400 to 0.1 Pa, and then returns to its initial value as ambient converts into air again. The increase of current is consistent with the increase of the t_{life} as a result of reduction of the oxygen readsorption rate in the oxygen-deficient environments after trapping holes. In particular, 0.1 Pa pressure eventually induces an obvious photoresponse decrease (t_r and t_d are 16.5 and 0.6 s, respectively), which evidences the contribution to photoresponse from photoinduced oxygen desorption and readsorption. This trapping process is further confirmed by light-intensity dependent QE in the following paragraph. 2) The one-dimensionality of the nanobelts can confine the active area of the charge carriers and, therefore, hinder the diffusion process, which results in a short t_{tran}. 3) High-quality single crystals facilitate the transport of carriers. Since $t_{tran} = l/v$, where l is the electrode distance (2.7 μm), the carrier drift velocity v is the product of mobility μ and applied electric field E, i.e., $v = \mu E$. Thus, QE can be rewritten as QE = $t_{life}\mu E/l$. The μ value is estimated as 4.9 cm^2 V^{-1} s^{-1} at room temperature for QE = 2.0 × 10^8%, t_{life} = 3.23 ms, and $E = 3.7 \times 10^4$ V cm^{-1}. Such a mobility value guarantees the effective transport of carriers between two electrodes. From the above presented analysis, the surface hole-trap states increase the t_{life} and the confined active area, and the availability of a high-quality single crystal leads to a reduction of t_{tran}, which significantly increases the ratio of t_{life}/t_{tran} and thus enhances the QE.

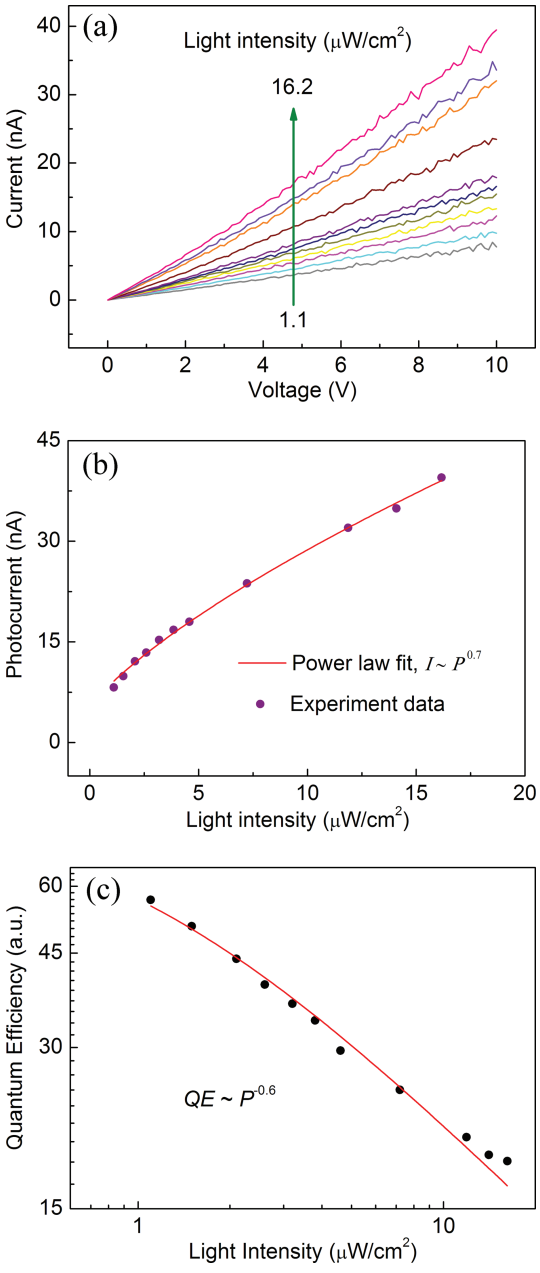

Figure 4. a) *I–V* curves of an $In_2Ge_2O_7$-nanobelt photodetector under 230 nm light irradiation of different intensities. b) Photocurrent as a function of light intensity and corresponding fitting curve using the power law. c) The light intensity-dependent QE of the $In_2Ge_2O_7$-nanobelt photodetector at the excitation wavelength of 230 nm at a bias of 10 V. The red solid line shows fitting of the experimental data to $QE \sim P^{-0.6}$.

The photoresponse of $In_2Ge_2O_7$ nanobelts is dependent on light intensity. **Figure 4a** shows the *I–V* curves of photodetectors irradiated by 230 nm light with varying intensity. The photocurrent increases with the light intensity, consistent with the fact that the charge carrier photogeneration efficiency is proportional to the absorbed photon flux. The corresponding dependence is plotted in Figure 4b. This can be fitted to a power law, $I_p \sim P^{\theta}$, where θ determines the response of the photocurrent to light intensity. The fitting gives nearly a linear behavior with $\theta = 0.7$. The non-unity ($0.5 < \theta < 1$) exponent suggests a complex process of electron–hole generation, recombination, and trapping within a semiconductor.[15] Furthermore, the contribution of traps can also be identified by the intensity-dependent behavior of the QE, as shown in Figure 4c. From this logarithmic plot, the $QE \sim P^{-0.6}$ relation shows a clear power law fitting in the intensity range. The decrease of the QE is a strong manifestation of hole-trap saturation for the relatively high light intensity. In addition, the onset of carrier bimolecular recombination at the highest light intensities may also contribute to shortening of the carrier lifetime.[16]

In conclusion, high-quality single crystalline $In_2Ge_2O_7$ nanobelts were synthesized by a vapor transport process. Individual $In_2Ge_2O_7$ nanobelts were designed for DUV solar-blind photodetectors. The detectors showed the high photoconductive performance, namely, high sensitivity and selectivity towards the solar-blind spectrum, excellent stability and reproducibility, fast response and decay times (~3 ms), and high responsivity (3.9×10^5 A W^{-1}) and quantum efficiency (2.0×10^8%). A power-law dependence of the nanobelt photocurrent on light intensity was determined. Based on the dependence of photocurrent on environment, and quantum efficiency on light intensity, the high performance of the $In_2Ge_2O_7$ nanobelts was ascribed mainly to surface traps, one-dimensionality, and high-quality single-crystal character. The present $In_2Ge_2O_7$ nanobelt photodetectors are envisaged to find wide optoelectronic applications in optical sensing, switches, and communication systems.

Experimental Section

Material Preparation and Characterization: $In_2Ge_2O_7$ nanobelts were synthesized by a vapor transport process in a horizontal tube furnace.[12d] In a typical experiment, a small quartz tube containing mixed GeO_2, In_2O_3, and carbon powder (molar ratio 2:1:4) was loaded into the furnace. Cleaned Si (100) substrates (without catalyst coating) were placed at the downstream end to collect the products. The temperature in the center of the furnace was increased to 1000 °C at a rate of 10 °C min^{-1} and maintained for 60 min. An Ar flow mixed with 5% O_2 at a total flow rate of 200 sccm (standard cubic centimeter per minute) was used as the carrier gas. The nanobelt growth temperature was in the range of 620–700 °C. The furnace power was then switched off and allowed to cool naturally to room temperature after the growth.

The as-prepared $In_2Ge_2O_7$ nanobelts were characterized by X-ray diffraction (XRD, Ultima IV/PSK), FE-SEM (Hitachi S-4800), and HRTEM (JEM-3000F).

Device Fabrication and Measurements: Individual $In_2Ge_2O_7$-nanobelt solar-blind photodetectors were assembled by a standard microfabrication process in a clean room. 1) The nanobelts were scraped from the substrate to disperse in ethanol, and then dropped on a Si substrate with a 200 nm SiO_2 layer. 2) The parallel microelectrodes were patterned on the top of the nanobelts using a standard optical lithography process divided into four steps: Firstly, Si substrates in (1) were covered with a photoresist by spin coating and then baked. Secondly, the photoresist was exposed to an intensive ultraviolet light through a pre-patterned mask. Thirdly, unused photoresist was removed by a special developer solution. After developing, a Cr/Au (10 nm/100 nm) film was deposited on the surface of the substrate in an electron beam deposition apparatus. Finally, a lift-off process produced the final nanodevice.

The current–voltage (*I–V*) characteristics of the photodetectors were measured using an Advantest Picoammeter R8340A and a dc voltage source R6144. A spectral response for different wavelengths was recorded using a 500 W Ushio xenon lamp with an illumination

bandwidth of 2 nm, and an Acton Research monochromator with order sorting filters was used. A photocurrent was measured by fixing certain light wavelengths with adjustable light intensity. The light intensity was modulated through an aperture and calibrated by using a UV-enhanced Si photodiode. A transient response was measured by using a 350 MHz Tektronix (TDS 5000B) oscilloscope with a 50 V impedance by illuminating the nanobelts with a 230 nm light pulse chopped at a frequency of 100 Hz.

Supporting Information

Supporting Information is available from the Wiley Online Library or from the author.

Acknowledgements

This work was supported by the International Center for Materials Nanoarchitectonics (MANA), National Institute for Materials Science (NIMS), Japan. X. S. Fang thanks the financial support from Grants-in-Aid for Scientific Research (B), JSPS (No. 22760517). The authors thank Dr. Hongqiang Wang in AIST for the optical absorption measurement.

Received: July 21, 2010
Published online: September 21, 2010

[1] Y. Taniyasu, M. Kasu, T. Makimoto, *Nature* **2006**, *441*, 325.
[2] M. Razeghi, A. Rogalski, *J. Appl. Phys.* **1996**, *79*, 7433.
[3] L. K. Wang, Z. G. Ju, J. Y. Zhang, J. Zheng, D. Z. Shen, B. Yao, D. X. Zhao, Z. Z. Zhang, B. H. Li, C. X. Shan, *Appl. Phys. Lett.* **2009**, *95*, 131 113.
[4] a) J. Xing, E. Guo, K. J. Jin, H. Lu, J. Wen, G. Yang, *Opt. Lett.* **2009**, *34*, 1675; b) M. Y. Liao, Y. Koide, J. Alvarez, *Appl. Phys. Lett.* **2007**, *90*, 123 507; c) Z. G. Ju, C. X. Shan, D. Y. Jiang, J. Y. Zhang, B. Yao, D. X. Zhao, D. Z. Shen, X. W. Fan, *Appl. Phys. Lett.* **2008**, *93*, 173 505.
[5] a) K. Koike, K. Hama, I. Nakashima, G. Takada, K. Ogata, S. Sasa, M. Inoue, M. Yano, *J. Cryst. Growth* **2005**, *278*, 288; b) T. Tut, T. Yelboga, E. Ulker, E. Ozbay, *Appl. Phys. Lett.* **2008**, *92*, 103 502; c) A. Soltani, H. A. Barkad, M. Mattalah, B. Benbakhti, J. C. De Jaeger, Y. M. Chong, Y. S. Zou, W. J. Zhang, S. T. Lee, A. BenMoussa, B. Giordanengo, J. F. Hochedez, *Appl. Phys. Lett.* **2008**, *92*, 053 501.
[6] a) T. Y. Wei, C. T. Huang, B. J. Hansen, Y. F. Lin, L. J. Chen, S. Y. Lu, Z. L. Wang, *Appl. Phys. Lett.* **2010**, *96*, 013 508; b) S. Liu, J. Ye, Y. Cao, Q. Shen, Z. Liu, L. Qi, X. Guo, *Small* **2009**, *5*, 2371; c) M. Law, H. Kind, F. Kim, B. Messer, P. Yang, *Angew. Chem. Int. Ed.* **2002**, *41*, 2405. d) Y. Yao, Y. Liang, V. Shrotriya, S. Xiao, L. Yu, Y. Yang, *Adv. Mater.* **2007**, *19*, 3979; e) L. Liao. B. Yan, Y. F. Hao, G. Z. Xing, J. P. Liu, B. C. Zhao, Z. X. Shen, T. Wu, L. Wang, J. T. L. Thong, C. M. Li, W. Huang, T. Yu, *Appl. Phys. Lett.* **2009**, *94*, 113 106; f) L. Li, P. C. Wu, X. S. Fang, T. Y. Zhai, L. Dai, M. Y. Liao, Y. Koide, H. Q. Wang, Y. Bando, D. Golberg, *Adv. Mater.* **2010**, *22*, 3161.
[7] a) R. S. Chen, S. W. Wang, Z. H. Lan, J. T. H. Tsai, C. T. Wu, L. C. Chen, K. H. Chen, Y. S. Huang, C. C. Chen, *Small* **2008**, *4*, 925; b) Q. Wan, E. Dattoli, W. Lu, *Small* **2008**, *4*, 451; c) S. Hinds, L. Levina, E. J. D. Klem, G. Konstantatos, V. Sukhovatkin, E. H. Sargent, *Adv. Mater.* **2008**, *20*, 4398; d) Y. Zhou, L. Wang, J. Wang, J. Pei, Y. Cao, *Adv. Mater.* **2008**, *20*, 3745; e) G. A. O'Brien, A. J. Quinn, D. A. Tanner, G. Redmond, *Adv. Mater.* **2006**, *18*, 2379.
[8] a) J. S. Jie, W. J. Zhang, Y. Jiang, X. M. Meng, Y. Q. Li, S. T. Lee, *Nano Lett.* **2006**, *6*, 1887; b) R. S. Chen, C. Y. Lu, K. H. Chen, L. C. Chen, *Appl. Phys. Lett.* **2009**, *95*, 233 119; c) S. Mathur, S. Barth, H. Shen, J. C. Pyun, U. Werner, *Small* **2005**, *1*, 713; d) K. Szendrei, F. Cordella, M. V. Kovalenko, M. Böberl, G. Hesser, M. Yarema, D. Jarzab, O. V. Mikhnenko, A. Gocalinska, M. Saba, F. Quochi, A. Mura, G. Bongiovanni, P. W. M. Blom, W. Heiss, M. A. Loi, *Adv. Mater.* **2008**, *21*, 683; e) X. S. Fang, Y. Bando, M. Y. Liao, U. K. Gautam, C. Y. Zhi, B. Dierre, B. D. Liu, T. Y. Zhai, T. Sekiguchi, Y. Koide, D. Golberg, *Adv. Mater.* **2009**, *21*, 2034; f) Y. Jiang, W. J. Zhang, J. S. Jie, X. M. Meng, X. Fan, S. T. Lee, *Adv. Funct. Mater.* **2007**, *17*, 1795.
[9] a) P. J. Li, Z. M. Liao, X. Z. Zhang, X. J. Zhang, H. C. Zhu, J. Y. Gao, K. Laurent, Y. L. Wang, N. Wang, D. P. Yu, *Nano Lett.* **2009**, *9*, 2513; b) H. W. Lin, S. Y. Ku, H. C. Su, C. W. Huang, Y. T. Lin, K. T. Wong, C. C. Wu, *Adv. Mater.* **2005**, *17*, 2489; c) C. Soci, I. W. Hwang, D. Moses, Z. Zhu, D. Waller, R. Gaudiana, C. J. Brabec, A. J. Heeger, *Adv. Funct. Mater.* **2007**, *17*, 632; d) Y. Wang, Z. Tang, P. Podsiadlo, Y. Elkasabi, J. Lahann, N. A. Kotov, *Adv. Mater.* **2006**, *18*, 518; e) H. Wu, Y. Sun, D. Lin, R. Zhang, C. Zhang, W. Pan, *Adv. Mater.* **2008**, *21*, 227; f) R. S. Chen, H. Y. Chen, C. Y. Lu, K. H. Chen, C. P. Chen, L. C. Chen, Y. J. Yang, *Appl. Phys. Lett.* **2007**, *91*, 223 106.
[10] a) P. Feng, J. Y. Zhang, Q. H. Li, T. H. Wang, *Appl. Phys. Lett.* **2006**, *88*, 153 107; b) C. Yan, N. Singh, P. S. Lee, *Appl. Phys. Lett.* **2010**, *96*, 053 108.
[11] a) T. E. Gier, X. H. Bu, P. Y. Feng, G. D. Stucky, *Nature* **1998**, *395*, 154; b) S. S. Bayya, G. D. Chin, J. S. Sanghera, I. D. Aggarwal, *Opt. Express* **2006**, *14*, 11 687.
[12] a) J. H. Zhan, Y. Bando, J. Q. Hu, L. W. Yin, X. L. Yuan, T. Sekiguchi, D. Golberg, *Angew. Chem. Int. Ed.* **2006**, *45*, 228; b) Y. Su, S. Li, L. Xu, Y. Q. Chen, Q. T. Zhou, B. Peng, S. Yin, X. Meng, X. M. Liang, Y. Feng, *Nanotechnology* **2006**, *17*, 6007; c) C. Yan, T. Zhang, P. S. Lee, *Cryst. Growth Des.* **2008**, *8*, 3144; d) C. Yan, N. Singh, P. S. Lee, *Cryst. Growth Des.* **2009**, *9*, 3697.
[13] T. Gacwdang, J. P. Chaminade, P. Gravereau, A. Garcia, C. Fouassier, M. Pouchard, P. Hagedrnuller, *Z. Anorg. Allg. Chem.* **1994**, *620*, 1965.
[14] a) C. Soci, A. Zhang, B. Xiang, S. A. Dayeh, D. P. R. Aplin, J. Park, X. Y. Bao, Y. H. Lo, D. Wang, *Nano Lett.* **2007**, *7*, 1003; b) A. Rose, Concepts in Photoconductivity and Allied Problems, Krieger Publishing Company, New York **1978**; c) Y. Takahashi, M. Kanamori, A. Kondoh, H. Minoura, Y. Ohya, *Jpn. J. Appl. Phys.* **1994**, *33*, 6611; d) L. Liu, C. R. Goria, S. Liang, N. Emanetoglu, Y. Lu, H. Shen, M. Wraback, *J. Electron. Mater.* **2000**, *29*, 69; e) E. Comini, A. Cristalli, G. Faglia, G. Sberveglieri, *Sens. Actuators B* **2000**, *65*, 260.
[15] H. Kind, H. Q. Yan, B. Messer, M. Law, P. D. Yang, *Adv. Mater.* **2002**, *14*, 158.
[16] C. Soci, D. Moses, Q. H. Xu, A. J. Heeger, *Phys. Rev. B* **2005**, *72*, 245 204.